Geometric Corrections on Sidescan Sonar Images based on Bathymetry. Application with SeaMARC II and Sea Beam Data

PIERRE CERVENKA[1], CHRISTIAN DE MOUSTIER[2], and PETER F. LONSDALE

Marine Physical Laboratory, Scripps Institution of Oceanography, University of California, San Diego, 9500 Gilman Drive, La Jolla, CA 92093-0205, U.S.A.

(Received 10 February 1993; Accepted 17 August 1993)

Key words: Bathymetry, Sidescan sonar, Pixel relocation, Acoustic backscatter image, Seafloor.

Abstract. Acoustic backscatter images of the seafloor obtained with sidescan sonar systems are displayed most often using a flat bottom assumption. Whenever this assumption is not valid, pixels are mapped incorrectly in the image frame, yielding distorted representations of the seafloor. Here, such distortions are corrected by using an appropriate representation of the relief, as measured by the sonar that collected the acoustic backscatter information. In addition, all spatial filtering operations required in the pixel relocation process take the sonar geometry into account. Examples of the process are provided by data collected in the Northeastern Pacific over Fieberling Guyot with the SeaMARC II bathymetric sidescan sonar system and the Sea Beam multibeam echo-sounder. The nearly complete (90%) Sea Beam bathymetry coverage of the Guyot serves as a reference to quantify the distortions found in the backscatter images and to evaluate the accuracy of the corrections performed with SeaMARC II bathymetry. As a byproduct, the processed SeaMARC II bathymetry and the Sea Beam bathymetry adapted to the SeaMARC II sonar geometry exhibit a 35m mean-square difference over the entire area surveyed.

1. Introduction

In seafloor surveys, classical sidescan sonars derive their information from the amplitude of echoes backscattered by the seafloor through a combination of the roughness of the water–seafloor interface, and of the geoacoustic properties of the bottom. Roughness is a multi-scale parameter defined with respect to the wavelength of the transmitted sound, and for most sidescan sonar systems, small scale (i.e. sizes of wavelength order) ranges from millimeters to decimeters, whereas large scale corresponds to dimensions from 10 m on up. As a result, large-scale seafloor features contribute highlights in the echo amplitude sequence, whereas the micro-roughness provides textural information in the sidescanned acoustic image of the seafloor.

In such images, the backscattered amplitudes are represented by pixels that are displayed as a function of time of arrival (slant range) or horizontal range in a raster format, where each scan line corresponds to one ping. Typically, pixels are square-shaped and have the same size throughout the scan line. However, the projection on the seafloor of the transmitted pulse, bounded by the sonar beam pattern, dictates that pixels should have an along-track versus across-track aspect ratio that increases away from nadir. The cross-track dimension of a pixel is proportional to the effective length of the transmitted pulse. It is several times smaller than its along-track extent which is a function of the horizontal width of the sonar beam pattern. Furthermore, the along-track extent of pixels in the raster image is constrained by the pulse repetition rate and by the forward speed of the platform.

The anamorphic distortion, introduced by forming the image with pixels of identical size and shape, is usually compensated to first order by appropriate duplication of scan lines in the display raster. However, when going from this relative raster format to a representation in geographic coordinates, as required for example when several tracks are merged into a mosaic, proper mapping of the echo amplitudes on the plane of the image becomes crucial.

The most common translation from slant ranges to athwartships horizontal ranges on a map relies

[1] Now at Laboratoire de Mécanique Physique, Universitité Paris VI, 78210 Saint-Cyr-l'Ecole, France.
[2] On leave at the Naval Research Laboratory, Code 7420, Washington D.C. 20375-5350.

Marine Geophysical Researches **16**: 365–383, 1994.

on a bottom represented by a horizontal plane referenced to the altitude of the sonar above the seafloor. Whenever the actual cross-track profiles of the seafloor relief differ from ideal flat horizontal lines, the result is distorted images that are potentially misleading for geomorphological interpretation. A number of methods have been devised to alleviate these distortions by modifying the horizontal plane assumption to a sloping plane, or preferably by using available bathymetry of the area derived from the same sonar system, e.g. SeaMARC II (Reed and Hussong, 1989; Stewart, 1989), Sys09 (Sternlicht, 1992) or from a gridded bathymetry data base (e.g. Sea Beam bathymetry with SeaMARC I (Lau and Fox, 1991), or Sea Beam bathymetry with GLORIA (Mitchell, 1991).

In this paper we present an analytical formulation of the mapping translation based on knowledge of the bathymetry in the area imaged, and of the acoustic radiation pattern of the sonar. The intent is to model the acoustic backscatter measurement geometry from the perspective of the sonar, and to use this geometry as a transfer function to reposition pixels within the image originally created using a flat horizontal bottom assumption. This process is only meant to bring pixels as close as possible to their true geographic position. Except where this pixel mapping process involves interpolations or compressions, it does not deal with the magnitude or grey level of pixels as done for example in the stochastic backprojection scheme developed by Stewart (1989).

The method is tested on sidescanned acoustic images of Fieberling Guyot, a submerged volcano rising about 4000 m above the surrounding seafloor in the Northeastern Pacific (32° 5 N, 128° W). These data were collected with the SeaMARC II bathymetric sidescan sonar system during a joint Sea Beam–SeaMARC II survey (de Moustier *et al.*, 1990). The sloping relief of the Guyot, helps highlight the distortions caused in the acoustic images by the flat bottom assumption. Post-processed SeaMARC II bathymetry and gridded Sea Beam bathymetry of the Guyot are used for the terrain model. In both cases, the bathymetries have spatial resolutions that are commensurate with the large-scale seafloor roughness observed in the image, and are roughly of the same order of magnitude. The Sea Beam bathymetry is used here as a reference because it covers roughly 90% of the Guyot and it is more accurate than SeaMARC II bathymetry. By comparing the output of the relocation process based on this reference bathymetry with that based on post-processed SeaMARC II bathymetry, we can obtain a quantitative measure of the performance of the method using SeaMARC II data alone. Although this pixel relocation technique has been developed for the SeaMARC II sonar system, it is generally applicable to other sidescan sonar systems provided bathymetric coverage of the area surveyed is available at an appropriate resolution.

A theoretical description of the pertinent geometries and of the processing method is given in Section 2. In Section 3, the technique is applied to SeaMARC II and Sea Beam data. Geological implications of the results are discussed in Section 4.

2. Theory

2.1. Sidescan Geometry

The geometry of the problem is depicted in Figure 1 where we define a right angle reference frame with axes x across-track, y along-track and z depth. The seafloor is insonified athwartships on either side of the sonar platform within a wide fan of fixed azimuthal width (e.g. 2°), whose footprint broadens with increasing range. The basic problem is to map the amplitude, $g(t)$, of the echoes backscattered by the seafloor according to classical geometric projections. In the slant range representation, the echoes are simply displayed linearly with time t, referenced to the instant the pulse was transmitted. Assuming a constant sound speed c through the water column (no refraction), the slant range $s(t)$ is:

$$s(t) = ct/2. \tag{1}$$

For a sidescanned acoustic image of the seafloor, data are displayed starting at the first bottom return, at time t_h, corresponding to the slant range, $s = h$, of the closest distance from the sonar to the insonified seafloor:

$$t_h = 2h/c. \tag{2}$$

This representation requires essentially no processing and the incoming data stream can be fed directly into a graphic line-scan recorder, in analog or digital form, to produce a real-time acoustic image. Such a display is very useful to monitor data acquisition, and it is sometimes the only output available for small sidelooking sonar units. However, it gives a distorted image of the seafloor.

To overcome this distortion, a model of the seafloor relief must be assumed. A horizontal plane

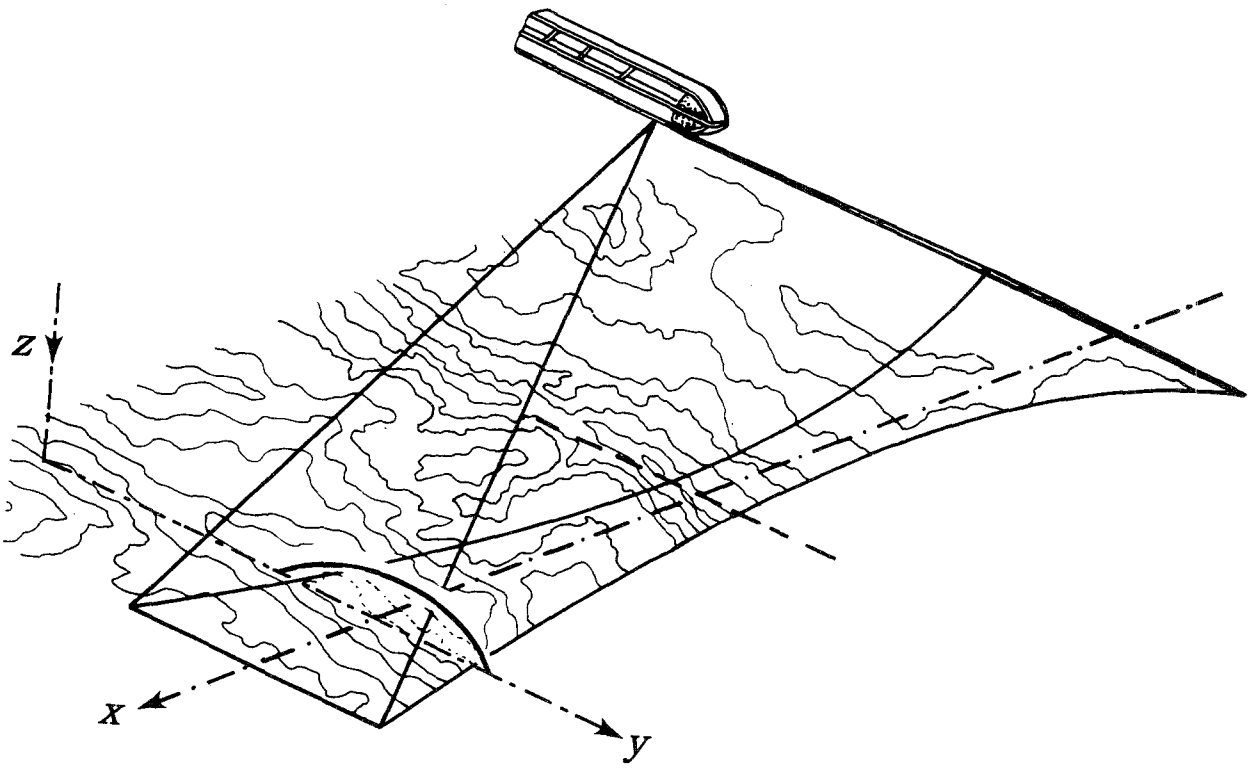

Fig. 1. Geometry of insonification. The beam footprint widens along-track away from nadir, implying that tappered windows of commensurate width should be used in along-track filtering operations. The coordinate reference frame is given by x across-track, y along-track and z depth.

is the simplest surface for this purpose, and its intersection with the assumed vertical plane of the sidescan acoustic beam is a straight horizontal line. The distance between this line and the sonar is the altitude, h, and the time series $g(t)$, recorded by the sonar during one ping, is viewed as the amplitude of echoes reflected by targets whose abscissa from nadir, $x(t)$, vary according to the elementary time law:

$$x(t) = \frac{c}{2}[t^2 - t_h^2]^{1/2}, \quad (t \geq t_h) \tag{3}$$

The horiontal scanning function $x(t)$ is monotonically increasing with time so that the grey levels $g(t)$ can be mapped isomorphically across-track according to $g(x)$. Displacements of pixels between the slant range and the horizontal range mapping are most pronounced in the near nadir region where $x(t)$ varies the fastest (Figure 2).

The time of first bottom return, t_h, is a critical parameter in the flat bottom geometry (Eq. 3). It varies along-track and must be determined for every ping either by analyzing the sidescan sonar signal itself, or through extrapolation of measurements made with independent devices (e.g. a 3.5 *kHz* subbottom profiler, etc.). Even for an ideal flat, horizontal seafloor, the finite time resolution of the bottom detection process and the constant sound speed assumption lead to inaccurate estimations of the altitude, h, resulting in a pixel positioning error δx. This error decreases with the athwartships distance, x, as shown by the approximation obtained by taking the derivative of Eq. (3) with respect to the first arrival time, t_h, and substituting for h in Eq. (2):

$$\delta x = -\frac{\delta h}{\tan \theta}, \tag{4}$$

where θ is the angle of incidence such that $\tan \theta = x/h$ (Figure 3). Eq. (4) is valid provided the relative position error remains small, i.e. $\delta x \ll x$. With this condition, Eq. (4) also applies to the more general cases where the lateral displacement δx is caused by a depth error $\pm\ \delta h$ when mapping the echo from a target area located in the incident direction θ (Figure 3).

When data have been displayed according to the flat bottom assumption, altitude corrections can be

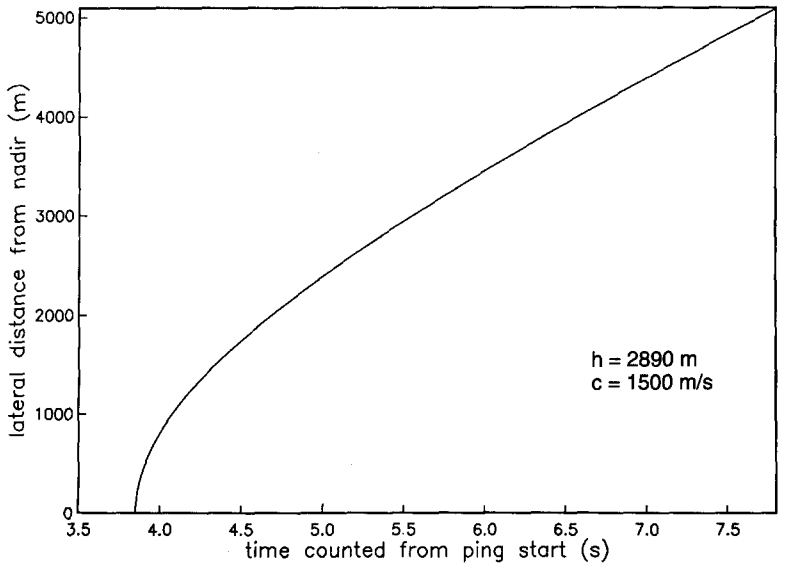

Fig. 2. Dynamic evolution of the lateral position of the pulse footprint on the seafloor (flat bottom assumption). In this example, the altitude of the fish is $h = 2890$ m, and the sound speed is constant, $c = 1500$ m/s.

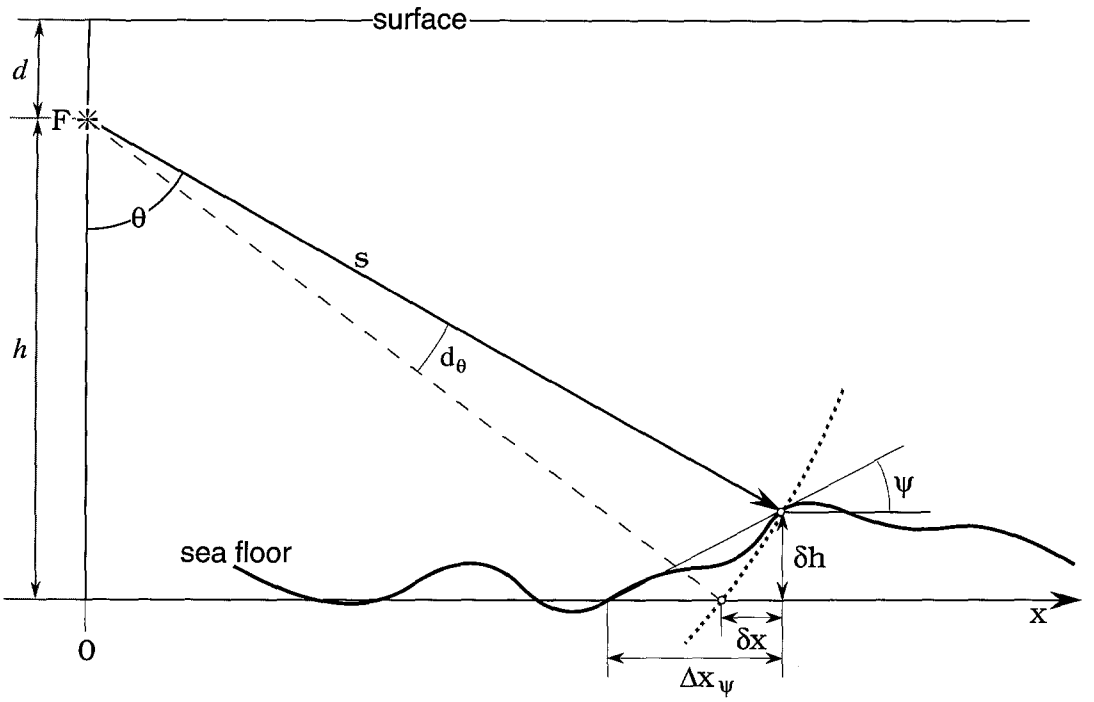

Fig. 3. Effect of seafloor slope on the position of pixels in the image. The x axis lies on the reference horizontal flat bottom. The sonar platform F is at altitude h above this plane, and depth d below the sea surface. The slant range s to the seafloor, with local slope angle ψ, is oriented at an angle θ from nadir. The seafloor profile can be locally described in parametric coordinates: $\psi(\theta)$.

applied during post-processing of the data. Improvements can be obtained by taking into account the true sound speed profile in the water column, and by smoothing the sequence of along-track altitudes, $h(y)$, over a number of pings. The underlying assumption is that, from one ping to the next, the small-scale variations of the altitude are not likely to be representative of the across-track relief aver-

aged over the swath width. Hence, the high spatial frequency components in $h(y)$ must be removed. This assumption is predicated on the fact that the sonar platform is decoupled from the heave motion of the towing ship. For deeply towed systems, that are directly attached to the tow cable, the ship's heave will contribute significant high-frequency components in $h(y)$ that must be taken into account before filtering $h(y)$. Altitude corrections are then translations applied on a ping-by-ping basis. The exact correction involves shifting each pixel from location x, calculated by using Eq. (3) with the original altitude h, to a new position $\bar{x}$, deduced from the same formula but with the filtered and/or corrected altitude $\bar{h}$:

$$\bar{x} = [x^2 + h^2 - \bar{h}^2]^{1/2}. \tag{5}$$

As a verification, the approximation given in Eq. (4) is consistent with this equation whenever $|\bar{x} - x| \ll |x|$.

For real-time display applications, it is usually convenient to represent the data according to a regular horizontal spatial sequence, with step Δx, that requires sampling the data with a variable-step sequence $t[i]$. From Eqs. (1–3), the corresponding sequence is written:

$$t[i] = [t_h^2 + (2i\Delta x/c)^2]^{1/2} \quad i = 0, 1, ..., n. \tag{6}$$

The resulting images are much less distorted than the direct slant range output. However, the method is based on the assumption that the along-track relief can be modeled by a ruled surface with horizontal generating lines. This assumption can be refined somewhat by modeling the relief with a ruled surface generated by straight lines whose slope may vary from one ping to the next. Then, for each ping the correction can be performed in two steps: (1) data are displayed on an inclined flat bottom profile, and (2) the resulting sequence is projected onto a standard horizontal map plane.

These 'flat bottom' methods are quite acceptable when the relief in the survey area is relatively smooth and when the slope estimations are well founded. As a result, large features are displayed at their correct location in the image. However, when the cross-track bathymetric profiles cannot be reasonably modeled by straight lines, distortions will still remain over extended areas.

Moreover, these corrections do not address the smaller features whose relief happens to be locally rough. A quantization of this phenomenon can be evaluated simply by considering a seafloor that is horizontal on average at the scale of a swath width, but rougher locally. Such a profile is described by means of the local bottom slope angles ψ, referenced to the elevation θ (Figure 3). The condition:

$$\psi < \theta \tag{7}$$

is assumed in this example to avoid the ambiguity problem which is addressed later. The local deformation $\varepsilon(\theta,\psi)$, representing the relative error made on the length of a small lateral segment Δx_ψ, when mapped with the idealized straight horizontal line approximation instead of the actual local slope, is equal to:

$$\varepsilon(\theta,\psi) = \frac{\delta x}{\Delta x_\psi} = \frac{\tan\psi}{\tan\theta}. \tag{8}$$

This relative error might not always be very small compared to unity. This means that, although large features might be properly located in the images, the textural information can be incorrectly displayed.

In this work, the images of seafloor acoustic backscatter amplitude are processed by using a more realistic and accurate seafloor surface model that takes into account a complete bathymetric representation of the area surveyed and the geometry of the sonar. This is achieved by performing a sequence of operations, described in greater detail in subsequent sections, starting with spatial filtering of the bathymetric data and transforming them to produce a relief model as viewed by the sidescan sonar. Then, data are processed on a ping-by-ping basis. The bathymetric profiles filtered across-track are analyzed to flag geometries responsible for simultaneous echoes from different targets. Each scan line of backscatter amplitude data is rearranged from the original array of equidistant pixels, sampled according to the flat bottom assumption, to a new array that is stretched and compressed according to the corresponding transformed bathymetric profile. Finally, this new array is interpolated to rebuild a regularly spaced scan line. At that point, the resulting relocated sonar image can be subjected to a variety of standard image processing techniques and merged with similarly processed adjacent tracks into a mosaic.

2.2. Processing Procedure

2.2.1. Bathymetry Conditioning and Filtering

A bathymetry map is normally used to describe the relief of a given region of the seafloor. In such a map, the accuracy and the meaning of each datum are closely related to the tools and techniques used

to acquire, process and present this information: the size of the incremental insonified area contributing to the instantaneous return and the spatial sampling density are pertinent parameters. However, for our intended application, the bathymetric data that we use are not meant to produce a user-oriented description of the relief. Rather, they are used to provide pertinent information on how the relief affects the time series of echo arrivals and hence their mapping in spatial coordinates.

Depending on the quality of the bathymetry data available, the first processing step usually consists of low-pass filtering the data to reduce its noise content. This is done across-track, using median filters plus convolutions with conventional tapered window functions (Hamming, 1973). Moreover, before entering the relocation algorithm, a careful data analysis must be performed to convert the bathymetric map into the relief actually sensed by the sonar. If the bathymetry data were low-pass filtered too severely, only large-scale features of the backscatter amplitude image would be relocated. Conversely, using small-scale bathymetry, whose resolution is far beyond that of the sidescan sonar, would produce irrelevant and incorrect pattern changes.

The instantaneous bottom echoes received at the arrays are backscattered by patches of seafloor that are each delimited across-track by the projection of the transmitted pulse on the bottom, and along-track by the horizontal width of the beam pattern of the acoustic arrays. The intersection of this beam pattern with the seafloor is a footprint whose along-track dimension increases with increasing slant range. Therefore, a pixel relocation scheme based on a bathymetry whose resolution is uniform across-track would not be consistent with the resolution of the arrays. The location of the corresponding pixels must be derived from a bathymetry that is convolved along-track with window functions whose length depends on the slant range and accounts for the horizontal width of the beam as well as the uncontrolled angular variations of the attitude of the fish (Figure 1). Consequently, the size of the window need not be very accurate, and the convolutions are not applied along contour lines defined by strictly constant slant ranges. Instead, for convenience they are applied at constant athwartships distances x, dividing the surveyed area into smaller portions whose relief is uniform enough to define an average altitude $\bar{h}$. Practically, we use parabolic tapered window functions whose length $w(x)$ equals:

$$w(x) = [x^2 + \bar{h}^2]^{1/2}\,\Theta_0\,. \tag{9}$$

Θ_0, expressed in radians, denotes the sum of the characteristic aperture of the azimuthal fan of the sonar (e.g. 1/20 radians for SeaMARC II) and an estimated upper limit on the angular variations due to the attitude (yaw, pitch ...) of the fish.

2.2.2. *Ambiguities*

After filtering by convolution with parabolic windows, the reconditioned bathymetric data are scanned again on a ping-by-ping basis. Individual profiles are analyzed to detect and flag geometries responsible for simultaneous echoes arriving from different parts of the profile. In the following, for each side the profiles are described by athwartships sequences of slant ranges $\{(s, x)_i\}$, or depths $\{(z, x)_i\}$, $i = 0,1, ..., n$. It is assumed that these sequences are properly ordered to follow the bathymetric profile, i.e.:

$$x_j \geq x_i \quad \text{whenever} \quad j > i. \tag{10}$$

Using the set $\{(s, x)\}$, a pair indexed i is part of an ambiguous portion of the profile if, and only if, another pair indexed j exists such that:

$$(s_j - s_i)\,(j - i) \leq 0 \quad (j \neq i). \tag{11}$$

Relocation of backscatter amplitude data coming from these areas is rather arbitrary, and the greater their lateral extent, the more arbitrary the result. However, depending on the bathymetry input, simply omitting the associated backscatter data would yield patchy images or it would remove large areas from the image.

To cope with these ambiguous areas but still display all the recorded backscatter data, the 'ambiguous' pairs found in a sampled profile are first discarded, thus providing monotonic sequences $\{(s, x)\}$. Then, interpolation between the remaining valid adjacent pairs can be applied as described in the next section. Interpolation between the valid boundaries of an ambiguous section of the profile (e.g. points A and B in Figure 4) seems to be the more natural option where the echoes of the temporal sequence are monotonically assigned to increasing lateral distances. Unfortunately, elementary geometrical considerations show that ambiguities are more likely to occur near nadir, a critical region where lateral shifts usually have the largest amplitude (Figure 2). Furthermore, there is no way to interpolate the backscatter amplitude data if nadir is part of the

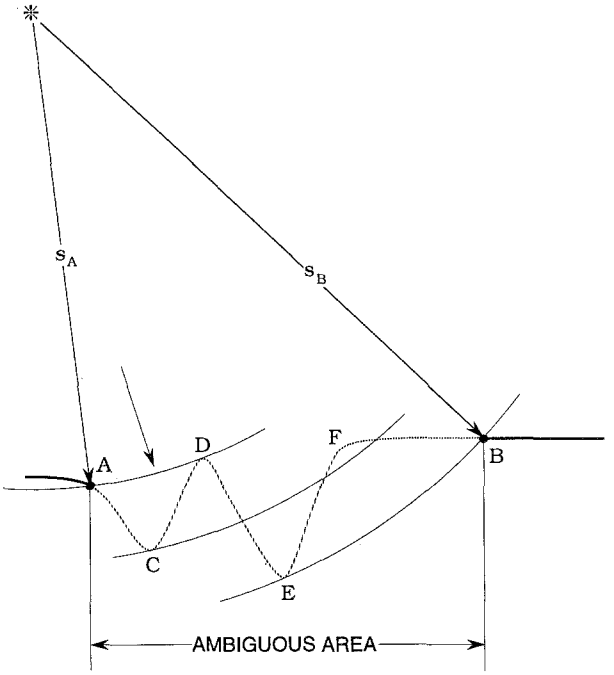

Fig. 4. Example of ambiguous area. Points A and B, at slant ranges s_A and s_B, respectively, bound a section of the bottom profile from which multiple synchronous echoes are received ($s_A = s_D \leq s_F \leq s_C < s_E = s_B$).

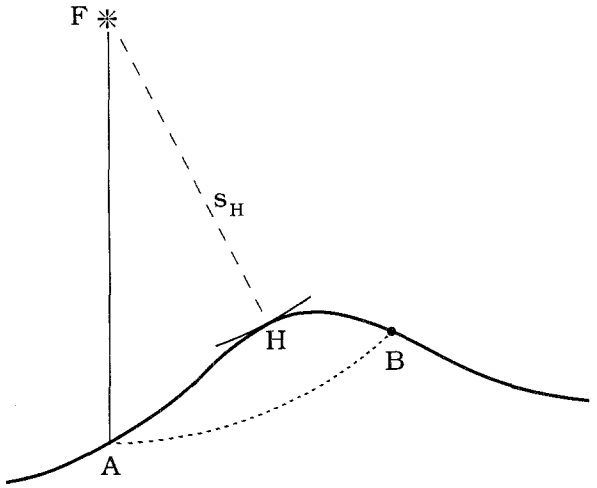

Fig. 5. Ambiguous area starting from nadir. A fictitious bathymetric profile includes segment FH. An interpolation scheme is then applied between point H and the first valid boundary B.

ambiguous area, because one of the valid boundaries is missing.

When an ambiguous area starts from nadir (Figure 5), we 'unfold' the sequence of backscattered echoes outward, beginning near the origin of the first bottom return, H (point of the bottom profile nearest the sonar). This is done automatically, by simply starting the bathymetric sequence at the position of the fish, F. This provides a robust algorithm, because the straight line FH is now part of the solution and the first backscatter amplitude data are always 'pushed' away from nadir and mapped according to the actual first step of interpolation lying between point H and the outward valid boundary, B.

When the profile is smooth enough, echoes coming from the nadir area contain a superposition of two segments of images, growing from the 'nearest' summit H, toward opposite directions HA and HB. There is no way to separate these two embedded image segments. Here, we have chosen to display at the correct location the outer portion, HB, that is contiguous with the remaining part of the image, although the ghost of the inner part, HA, may be also perceived.

2.2.3. *Pixel Relocation, Interpolation Scheme*

The previous step yields complete sequences $\{(s, x)_i\}$ that are montonic and strictly positive, i.e.:

$$x_j \geq x_i \quad \text{and} \quad s_j > s_i \quad \text{whenever} \quad j > i. \tag{12}$$

To tie the backscatter amplitude data to these sequences, an interpolation scheme is required. Here, the speed of sound in the water column is still assumed to be constant, so that ray paths are straight lines. Every pixel sampled at time, t, is assumed to be representative of a target M, located at the corresponding slant range $s(t)$ given by Eq. (1). As illustrated in Figure 6, the lateral location x_M of this pixel is interpolated between the two nearest elements, $M_1 = (s, x)_1$ and $M_2 = (s, x)_2$, of the bathymetric sequence such that:

$$s_1 < s < s_2. \tag{13}$$

An easy and natural implementation of this scheme consists in performing linear interpolations directly in the (x, z) plane (Figure 6), i.e. assuming straight lines between elements of the $\{(z, x)\}$ sequence. This operation involves finding the abscissa, x_M, of the intersection, M, between the segment $[M_1M_2]$ and the circle of radius s centered at the fish location F. This requires solving the quadratic equation:

$$\begin{aligned}(s^2 - x_M^2)^{1/2}(x_2 - x_1) - x_M(z_2 - z_1) \\ = x_2(z_1 - d) - x_1(z_2 - d),\end{aligned} \tag{14}$$

in which d is the depth of the sonar. This is equivalent to the method used by Lau and Fox (1991) to

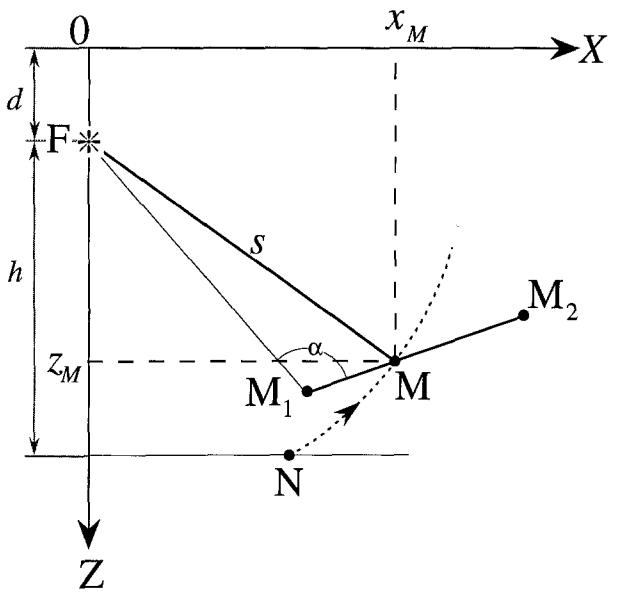

Fig. 6. Geometry of the pixel relocation process in the (x, z) plane. In the flat bottom assumption, an echo with slant range s, received by the sonar at altitude h above the bottom, comes from point N. If the seafloor is not flat, the pixel is relocated to point M with lateral location x_M derived by linear interpolation between the two nearest available points M_1 and M_2 whose slant ranges are such that $s_1 \leq (s = FM) \leq s_2$, which is verified whenever $\alpha \geq \pi/2$.

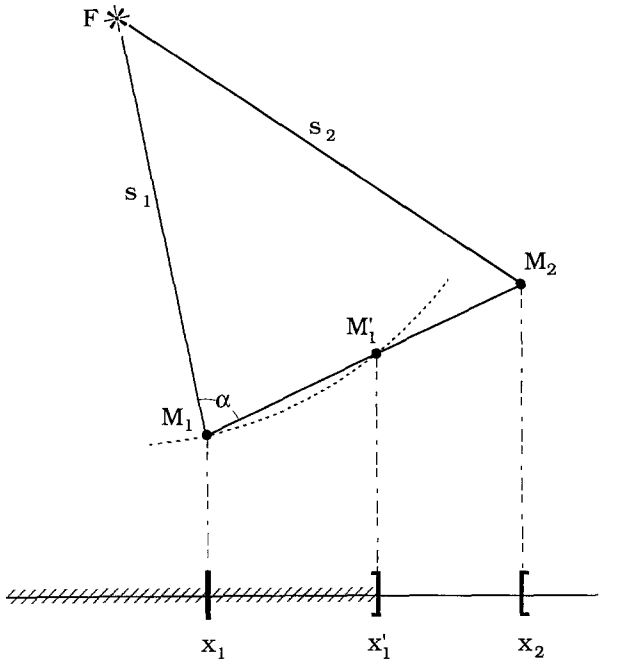

Fig. 7. Limits of the linear interpolation geometry of Figure 6 when $\alpha < \pi/2$. The segment $]M_1M_1'[$ corresponds to slant ranges that are always shorter than s_1. This case must be solved in the (x, s) plane as shown in Figure 8.

process SeaMARC I data with Sea Beam bathymetry.

However, this interpolation scheme is not always valid. Eq. (12) implies that angle FM_1M_2 is always greater than angle FM_2M_1, but Figure 7 shows that whenever angle FM_1M_2 is smaller than $\pi/2$, the slant range of any point on the chord M_1M_1' along the secant $]M_1M_2[$ of the circle of radius s_1, is smaller than s_1. Consequently, performing the interpolation in the (x, z) plane will necessarily relocate all points with slant range s satisfying Eq. (13) in the portion $]M_1'M_2[$ of the original segment. This will yield a gap over $]M_1M_1'[$ appearing as an artifact in the image. In such a case, the linear interpolation must take place in the (x, s) plane (Figure 8). This is always possible because the sequence $\{(s, x)\}$ is strictly monotonic. The pixel position is then simply defined by:

$$x_M = \frac{(x_2 - x_1)s + x_1 s_2 - x_2 s_1}{s_2 - s_1}. \qquad (15)$$

This process amounts to describing the profile between points M_1 and M_2 in the (x, z) plane by

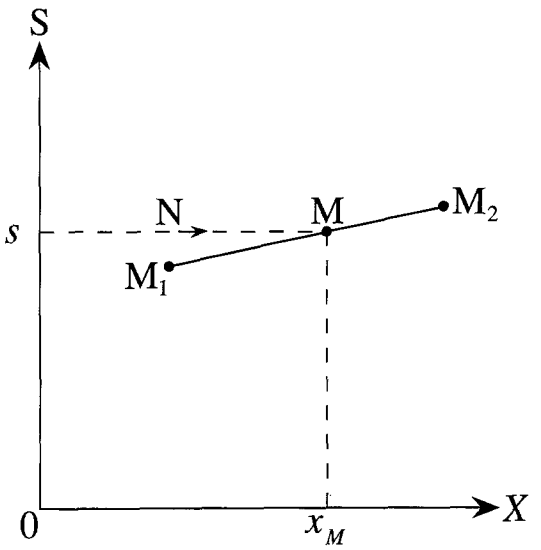

Fig. 8. Geometry of the pixel relocation process in the (x, s) plane used when the angle α defined in Figure 6 is less than $\pi/2$.

means of a portion of ellipse whose equation is:

$$\frac{(x - x_0)^2}{R_x^2} + \frac{(z - d)^2}{R_z^2} = 1,$$

with

$$R_z^2 = x_2 s_1 - x_1 s_2,\ R_x = \frac{(x_2 - x_1)R_z^2}{(x_2 - x_1)^2 - (s_2 - s_1)^2},$$

$$x_0 = \frac{(s_2 - s_1)R_z^2}{(x_2 - x_1)^2 - (s_2 - s_1)^2}. \qquad (16)$$

Although processing in the (x, s) plane looks more convenient because it can be applied in every case and because the computation of Eq. (15) is easier than the solution of Eq. (14), these portions of ellipse introduce a slight 'wavy' distortion over areas where Eq. (14) applies (e.g. a flat bottom). Hence, Eq. (15) is only used in the few cases for which it is actually needed, and the profile domain (x, z) is preferred otherwise.

3. Application to SeaMARC II Data

The theory developed above is applied to data collected over Fieberling Guyot, where SeaMARC II data were recorded concurrently with Sea Beam bathymetry which, combined with additional Sea Beam bathymetry available from earlier surveys, provided 90% coverage with multibeam bathymetry data.

Fieberling Guyot is a 4 km-high extinct volcano in the Pacific basin 800 km west of San Diego (Carsola and Dietz, 1952). Hotspot volcanism built this feature above sea-level about 20 m.y. ago, as an island on the flank of the Miocene East Pacific Rise (Lonsdale, 1991). Its summit was planed off by subaerial and littoral erosion, and has subsided so that its shallowest point is now at a depth of 438 m. The Sea Beam bathymetry (Figure 9) shows that the side-slopes below the 650–750 m deep rim of the summit plain have concave profiles; average gradients decline from 20–30° in the upper kilometer to 7–15° at depths of 3000–4000 m. The relief of the side-slopes is complicated by numerous spurs and rows of secondary cones inferred to have grown along flank rift zones, by isolated parasitic cones, and by a submarine canyon network which leads down to a sediment fan on the north side of the Guyot. A thick sediment apron surrounds the Guyot, in some sectors completely filling the encircling structural moat. Seismic reflection profiles record sediment thicknesses of more than 500 m at the inner part of the apron, contrasting with the 100–150 m thick pelagic cover of the abyssal hill terrain beyond its outer margins. The generally smooth surface of this apron is interrupted by several sediment-covered satellite cones (Figure 10).

3.1. SeaMARC II Data

The SeaMARC II system is described in detail elsewhere (e.g. Blackinton, 1986); here we only recall the parameters pertinent to the processing described below. This shallow tow, long-range bathymetric sidescan sonar system outputs images of seafloor acoustic backscatter amplitude over a swath 10 km wide, and bathymetry over a swath whose width is the lesser of 3.4 times the altitude of the fish above the seafloor, or 10 km. The bathymetry is limited to roughly 60° from vertical down by the onset of the first bottom multiple which, in most cases, overcomes bottom echoes from the outer angles and invalidates the corresponding differential phase measurements used to derive such angles. Likewise, the sea surface reflection of the nadir bottom returns causes similar interferences in the phase data and, due to the comparatively large area insonified by the pulse near nadir, bathymetry is usually not reliable in the central region bounded by nadir and the surface reflection multiple. As a result, the bathymetry swath exhibits a central gap covering roughly $\pm 16°$ about vertical for a tow depth of 100 m. The gap decreases with tow depth.

A similar gap is found in the sidescanned acoustic images. Assuming a flat horizontal bottom, for a given transmitted pulse of length τ (e.g. 1 ms for SeaMARC II), as mentioned above the nadir bottom return comes from a region bounded by the intersection of a spherical shell, of thickness $c\tau/2$, with a plane. This return is inherently ambiguous because the region spans both sides of vertical and is much larger than the spatial resolution of the pulse once it propagates along the bottom interface. In order to avoid this problem, the first 40 samples after bottom detection are skipped. Each backscatter amplitude record consists of 984 pixels per side, sampled according to Eq. (6) which assumes a flat bottom and a fixed horizontal step (e.g. $\Delta x = 5$m). Therefore the acoustic image is made of two rectangular strips separated by a central gap roughly 400 m wide. The altitude and the depth of the fish are recorded in an 'attitude' file, which contains also other information such as time stamps and system engineering parameters.

For SeaMARC II bathymetry, an athwartships bottom profile is created for each ping as a sequence of (z, x) pairs where the depth z and the lateral distance x have been computed from range and elevation values given by the sonar. These profiles are not equally sampled athwartships and,

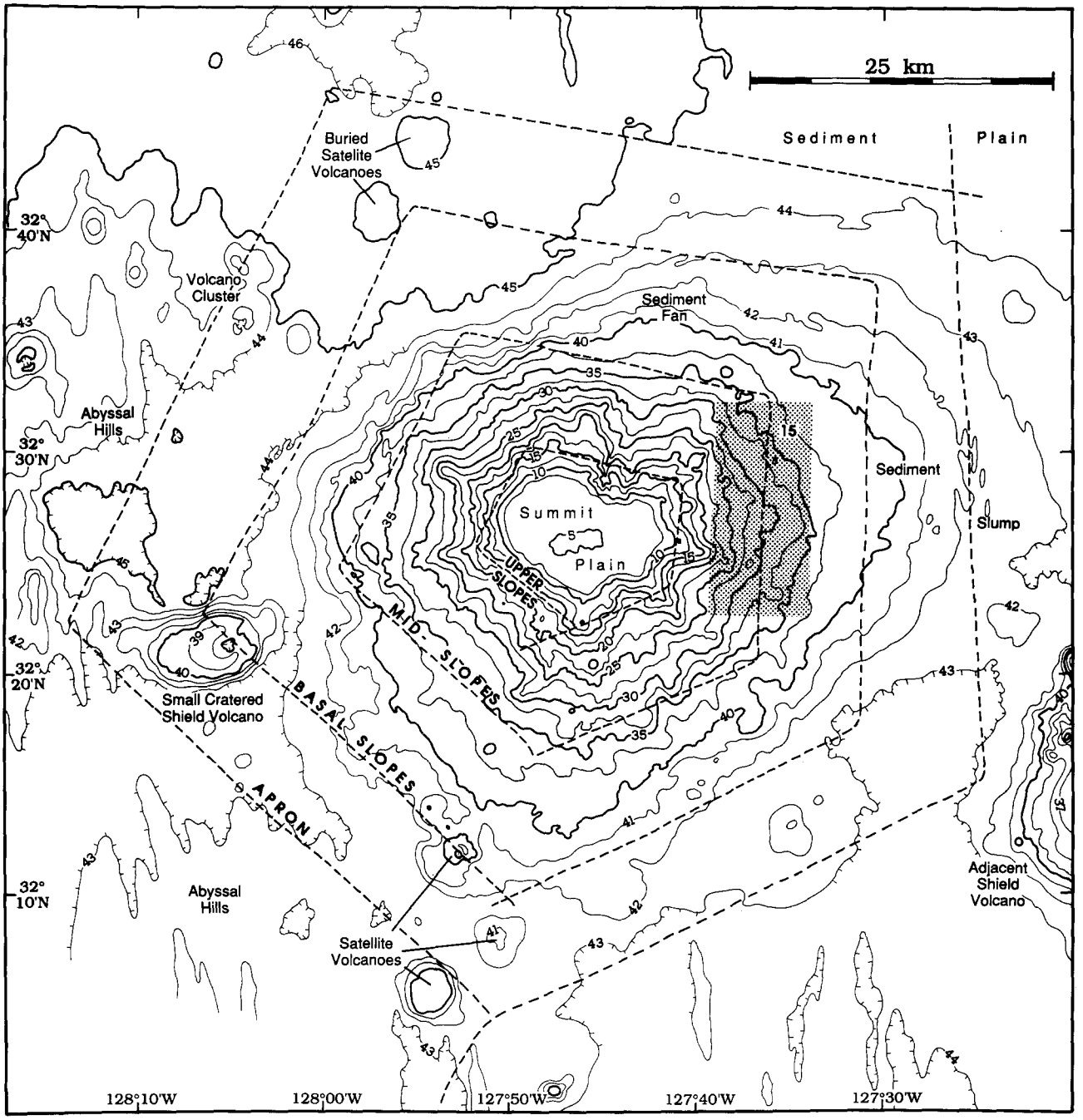

Fig. 9. Bathymetry of Fieberling Guyot displayed at 100 m contour intervals showing the track (dashed line) of the SeaMARC II sidescan survey displayed in Figure 10, and identifying the location (stippled area) of the image segment used to illustrate the results of the processing techniques presented (Figure 15).

as mentioned above, data are usually not available over the entire backscatter amplitude image. Moreover, the number of samples (typically 100 pairs per side) and the z-variations between adjacent pairs are not representative of the actual accuracy or reliability of these data. This original bathymetry is usually too noisy and must be processed. In this paper, this processing involves a selection of valid data points based on confidence criteria, decimation, regridding on a rectangular array, interpolation of nadir values, extrapolation of gaps in the coverage, and low-pass filtering across-track. In addition, along-track filtering is performed as described in Section 2.2. Figure 11a shows the ba-

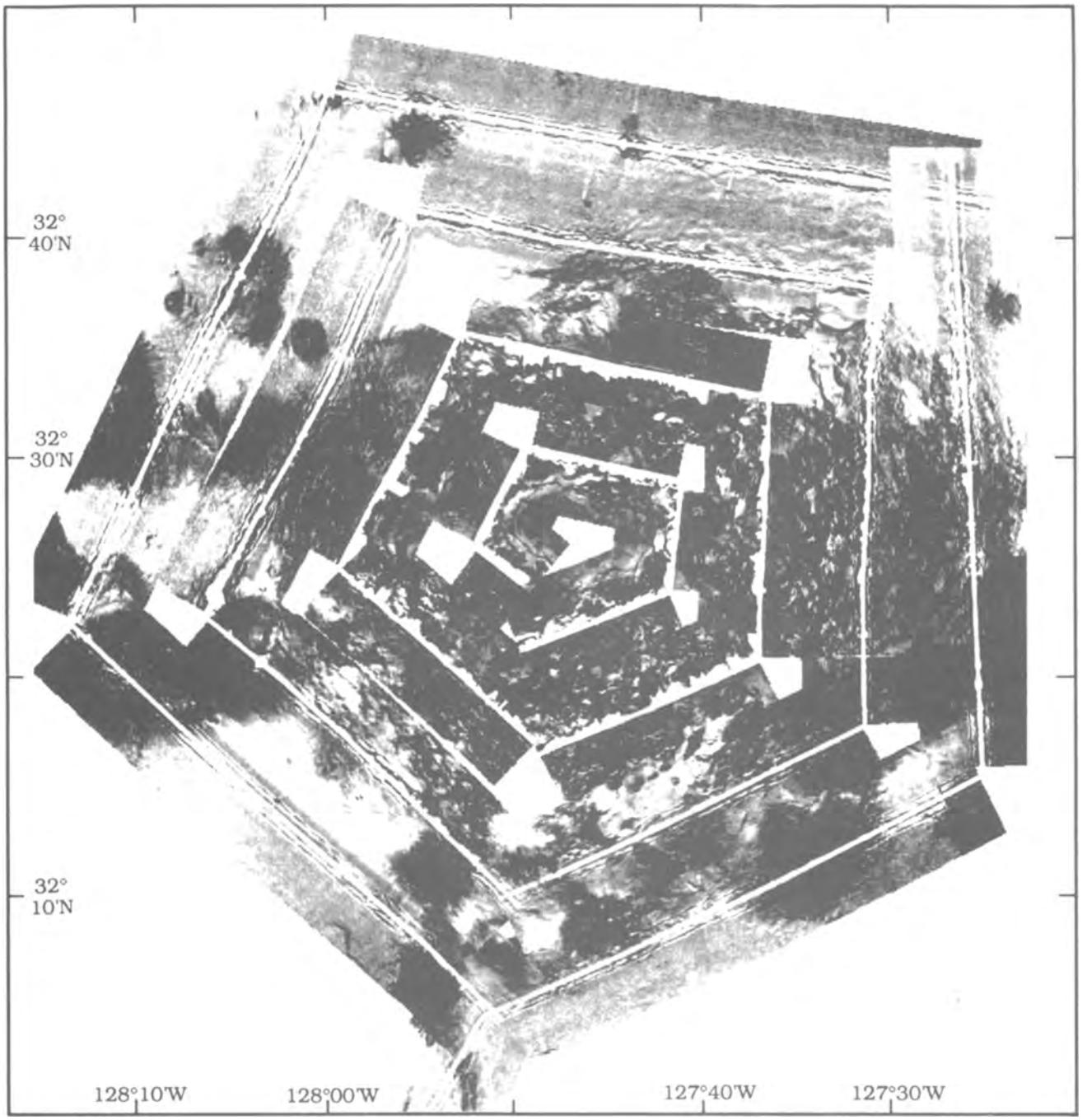

Fig. 10. SeaMARC II sidescan mosaic of Fieberling Guyot. Pixels in this image have been relocated based on Sea Beam bathymetry transformed to reflect the sidescan geometry. Contrast enhancement and image processing techniques applied are described in Cervenka and de Moustier (1993).

thymetry that is obtained after such processing but the areas to be extrapolated are left blank. Navigation is not taken into account (rectangular format), and each horizontal line is an athwartships profile that matches the corresponding backscatter amplitude raster line.

At Fieberling Guyot, SeaMARC II bathymetric and backscatter amplitude data were collected on

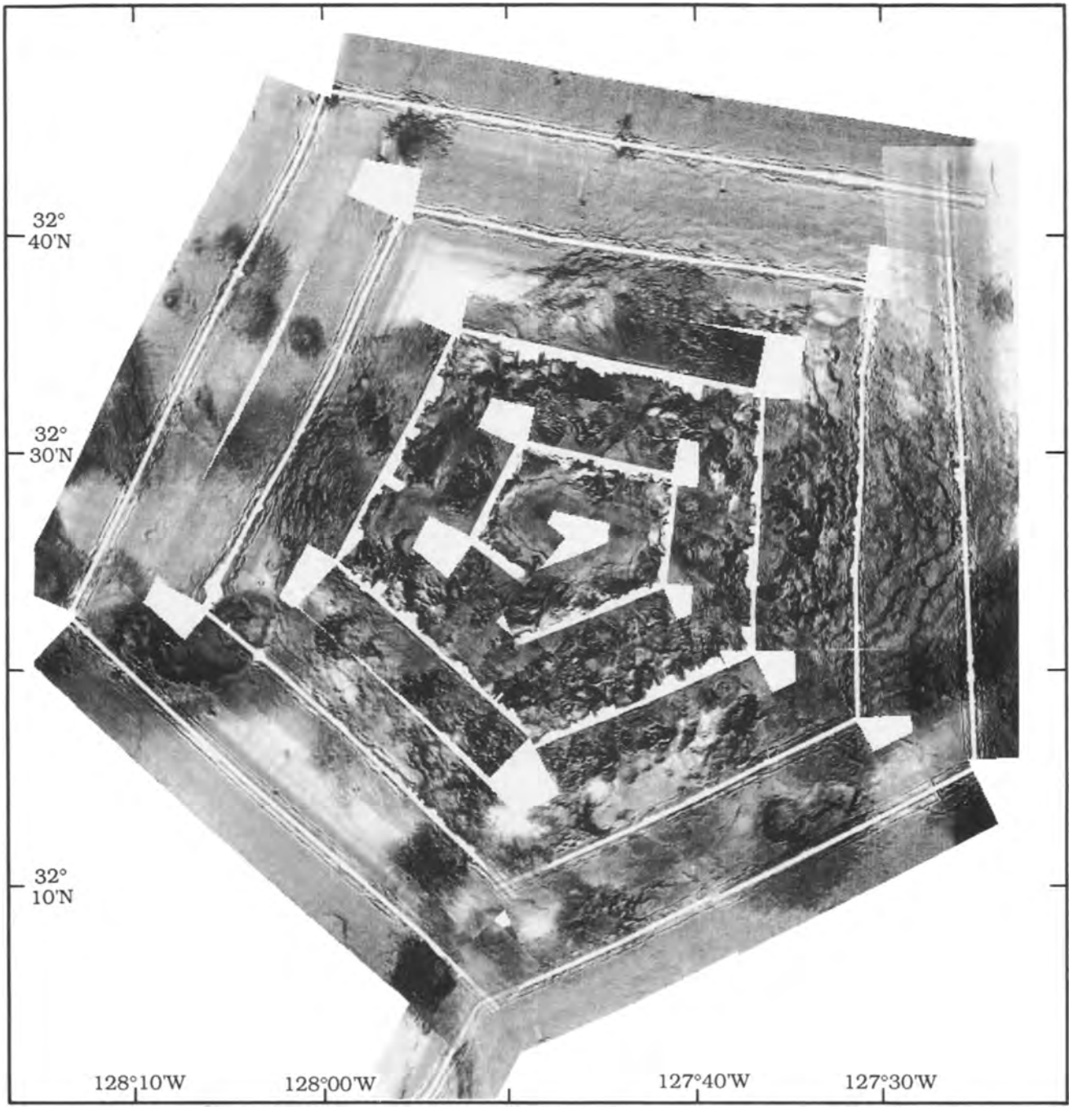

Fig. 10. SeaMARC II sidescan mosaic of Fieberling Guyot. Pixels in this image have been relocated based on Sea Beam bathymetry transformed to reflect the sidescan geometry. Contrast enhancement and image processing techniques applied are described in Cervenka and de Moustier (1993).

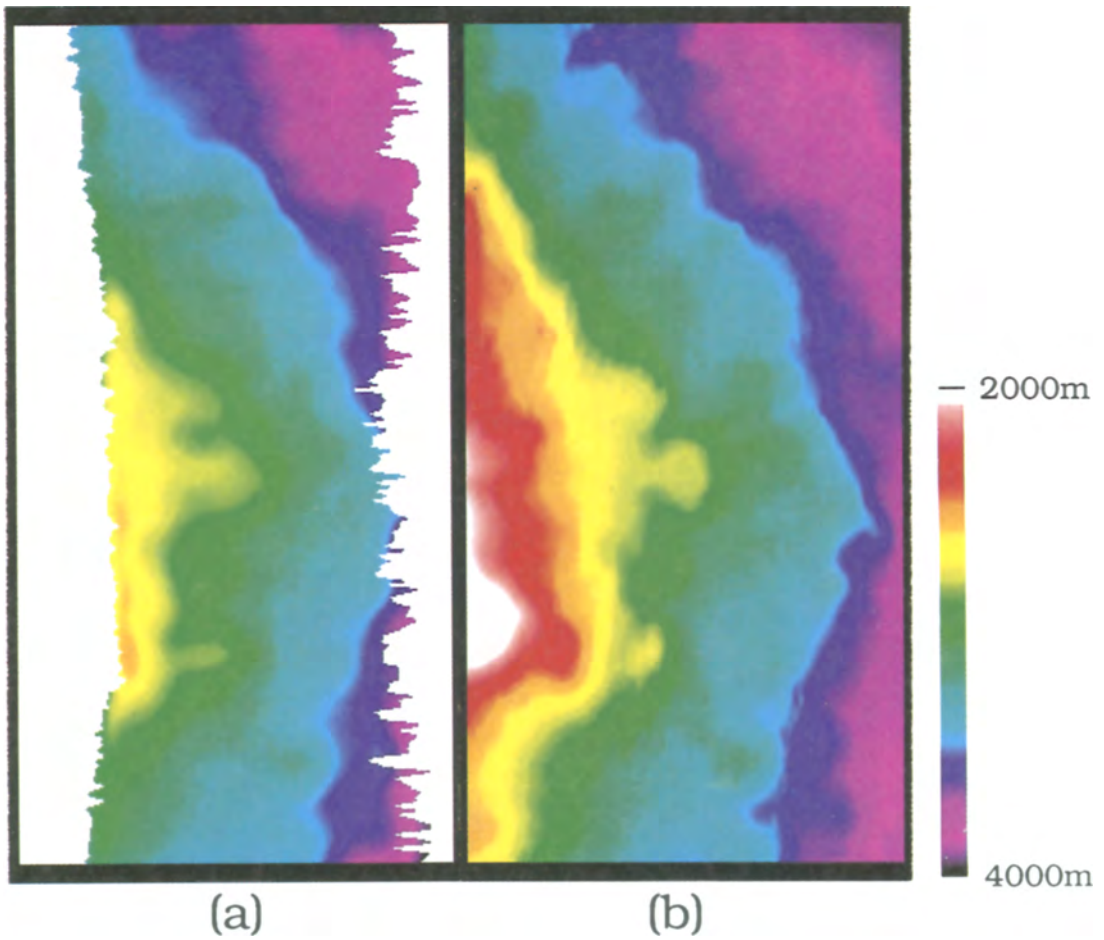

Fig. 11. Bathymetry of a segment of the flank of Fieberling Guyot. (a) Processed SeaMARC II bathymetry: The display is cropped at the original outer limits of the data. (b) Sea Beam bathymetry: A rectangular array is built by flying a fictitious but theoretically exact bathymetric sidescan system over Sea Beam bathymetry gridded with square cells 200 m wide. The color scale bar represents a depth range of 2000 m.

tracks spaced 10 km apart in a nested pentagonal pattern, over the upper slopes of the volcano at an average depth of 2000 m, the mid-slopes at 3500 m, the basal slopes at 4200 m and the apron at 4300–4600 m (Figures 9 and 10).

3.2. Sea Beam Data

As nearly complete Sea Beam coverage of Fieberling Guyot was available, the corresponding bathymetry has been used here in the pixel relocation process. The multibeam geometry of Sea Beam produces up to 16 pairs of depth and horizontal distance with beams roughly 2.7° wide, yielding depth estimates with accuracies of about 10 m rms (Renard and Allenou, 1979). The original Sea Beam data have been regridded with square cells 200 m wide. This size is consistent with the lower limit of the lateral resolution of the system given by the footprint of each beam at the average maximum depth (4000 m) in this region. Such a sampling density is also higher than the ultimate horizontal resolution derived from SeaMARC II bathymetry because the original real-time sequences of (z, x) pairs computed by the system must be edited on a ping-by-ping basis to retain only data whose slant ranges increase monotonically across-track from nadir out (Cervenka and de Moustier, submitted). This decimation process is predicated by the sidescan sonar geometry that cannot resolve echoes arriving simultaneously from different directions. Hence, in areas with more than a few hundred meters of relief across the swath, this edited SeaMARC II bathymetry is usually sparser and more uneven than the original real-time sequence.

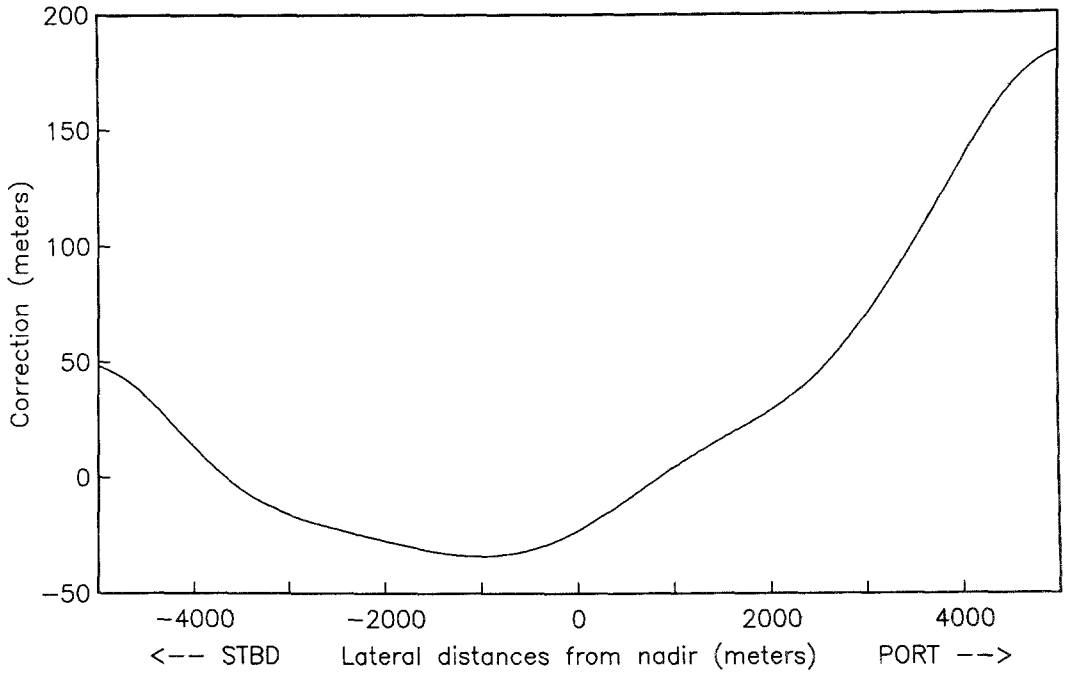

Fig. 12. Systematic correction applied on SeaMARC II bathymetric profiles. Correction toward shallower values are counted positive.

In order to apply the gridded Sea Beam bathymetry to the pixel relocation process, it must be transformed to be representative of the relief as seen by the SeaMARC II sonar arrays. To this end, it has been convenient to resample the Sea Beam grid into the SeaMARC II format covering the full image swath whenever possible. This was done by using the attitude and position of the tow fish to 'fly' it above the grid and sample a 10-km swath. The lateral x-spacing was uniform and with 128 points across the swath, the data were oversampled with regard to their actual information content (Figure 11b).

3.3. Comparison of Bathymetries

A meaningful comparison between Sea Beam and SeaMARC II bathymetries can only be performed provided the latter is further corrected to remove systematic errors. An important step in the process used to compute SeaMARC II bathymetry involves a table to convert electrical angles to elevation angles. This table is built on a statistical basis over an area assumed to be a horizontal plane. Because of the large depth differences (over 4000 m) existing in the survey area, such a table computed on the seafloor at the base of the Guyot is obviously inappropriate and is responsible for consistent across-track biases. In an effort to approach a zero mean difference between Sea Beam and SeaMARC II bathymetries and still simulate a correct conversion table, the average difference profile over the whole Guyot has been calculated (Figure 12) and subtracted from the SeaMARC II bathymetry data. Despite its empirical nature, this method manages to reduce the mean difference to a few meters. A quantitative estimate of the relative accuracy of the SeaMARC II bathymetry is then given by the mean square difference between the two processed bathymetries. The result is about 35 m rms over the whole Guyot.

3.4. Pixel Shifts and Image Reconstruction

An example of a SeaMARC II sidescan image whose pixels are displayed using a flat bottom assumption is shown in Figure 13a. This image is still in a rectangular format, i.e. without corrections taking into account navigation information. On the other hand, various image enhancements described elsewhere (Cervenka and de Moustier, 1993) have been applied: across- and along-track median filtering, destriping, compensation for systematic across-track variations due to incorrect time varying-gain or angle varying gain, and contrast enhancement.

The original recorded backscatter amplitude data have been sampled according to the flat bottom methodology described in Section 2. As a first

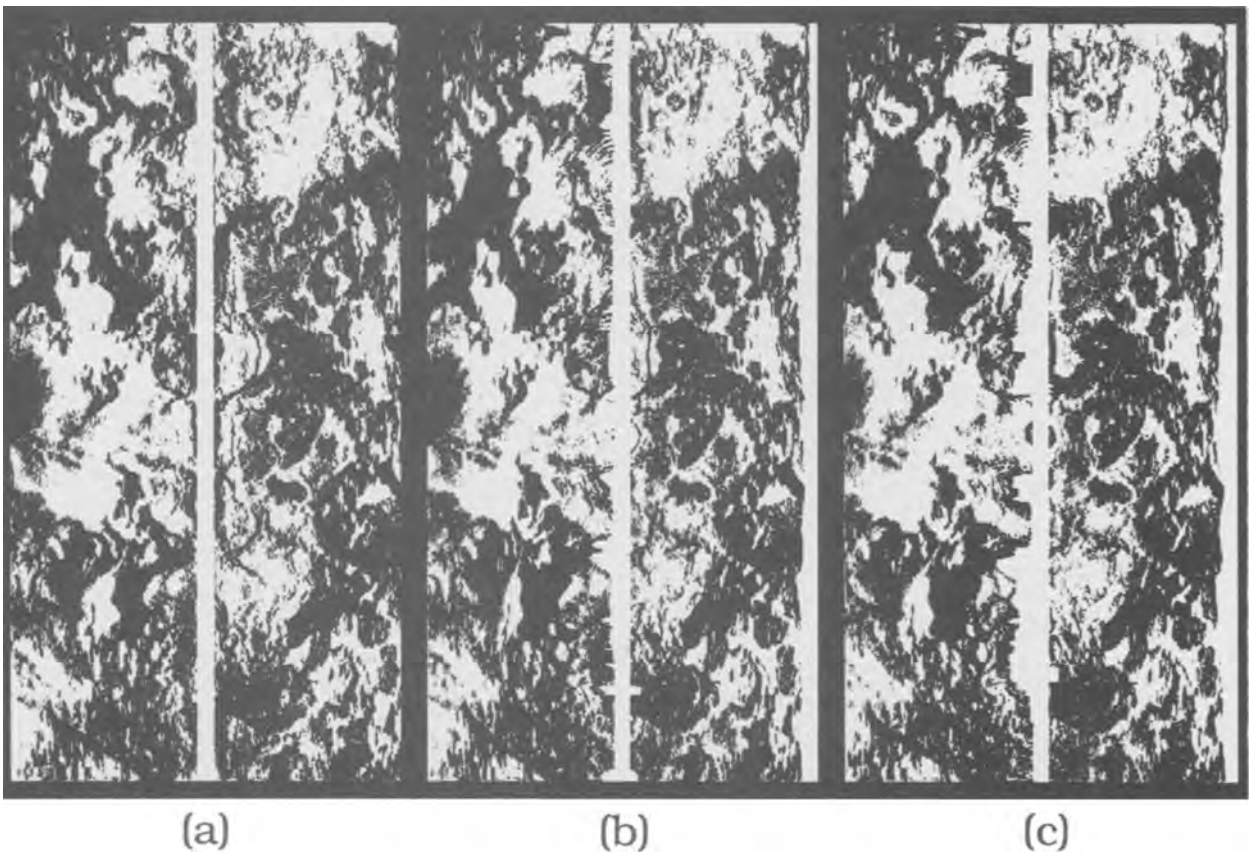

Fig. 13. SeaMARC II backscatter image of a middle slope segment of Fieberling Guyot (Figure 10). The image is contrast enhanced, but not navigated. The corresponding terrain slopes up on the left side of the track and down on the right side. (a) Pixels displayed with the original flat bottom assumption; (b) Pixels relocated according to SeaMARC II bathymetry; (c) Pixels relocated with transformed Sea Beam bathymetry as viewed by SeaMARC II.

step in the pixel relocation process an inversion from horizontal range to slant range (Eq. (6) and Eq. (1)) is performed to find the actual mapping of the original data. Pixels are then relocated and interpolated according to the methods presented in Section 2.2.3. The resulting lateral shifts are smoothed by convolution with a [1/4, 1/2, 1/4] window, before computing the final grids. Such low-pass filtering is justified by the finite duration along which the signal is integrated to determine the intensity of each pixel. This limits the largest variations occurring in the pixel relocation and reduces occasional intense moiré effects that might occur in areas of the corrected image that were stretched the most.

To monitor the effects of the terrain model in the pixel relocation process, a mapping of the pixel migrations is stored with the same format as that used for the backscatter amplitude data. Figure 14 presents a comparison of pixel migration results obtained for a single swath (Figure 13) with edited SeaMARC II bathymetry (Figure 14a) or with Sea Beam bathymetry transformed to SeaMarc II characteristics as described above (Figure 14b). The difference between these two mapping functions is shown in Figure 14c, indicating that most of the discrepancies are found in the near nadir area where large variations are more likely to occur as predicted by Eq. (4). As expected, discrepancies are also noticeable in the outer parts of the swath where SeaMARC II bathymetry is not available and where a linear horizontal extrapolation from the last valid sample has been applied.

Once the corrected horizontal locations of the recorded data have been assigned, the image is rebuilt with equi-spaced pixels. This is done by projecting the relocated values onto the original grid using linear interpolations. Relocated data that are compressed within a smaller interval than the elementary step are replaced by their average. Pixels moved outside of the outer limits are discarded. In principle, pixels that have been migrated towards

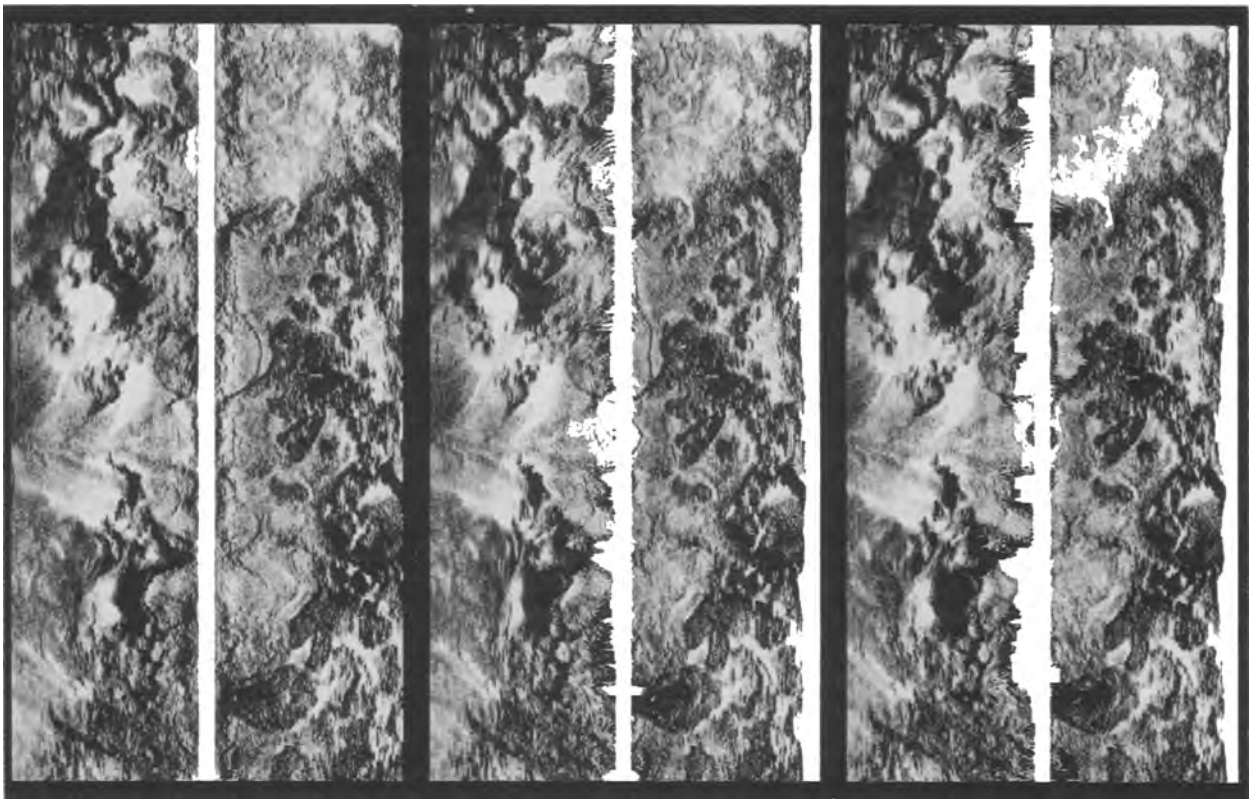

Fig. 13. SeaMARC II backscatter image of a middle slope segment of Fieberling Guyot (Figure 10). The image is contrast enhanced, but not navigated. The corresponding terrain slopes up on the left side of the track and down on the right side. (a) Pixels displayed with the original flat bottom assumption; (b) Pixels relocated according to SeaMARC II bathymetry; (c) Pixels relocated with transformed Sea Beam bathymetry as viewed by SeaMARC II.

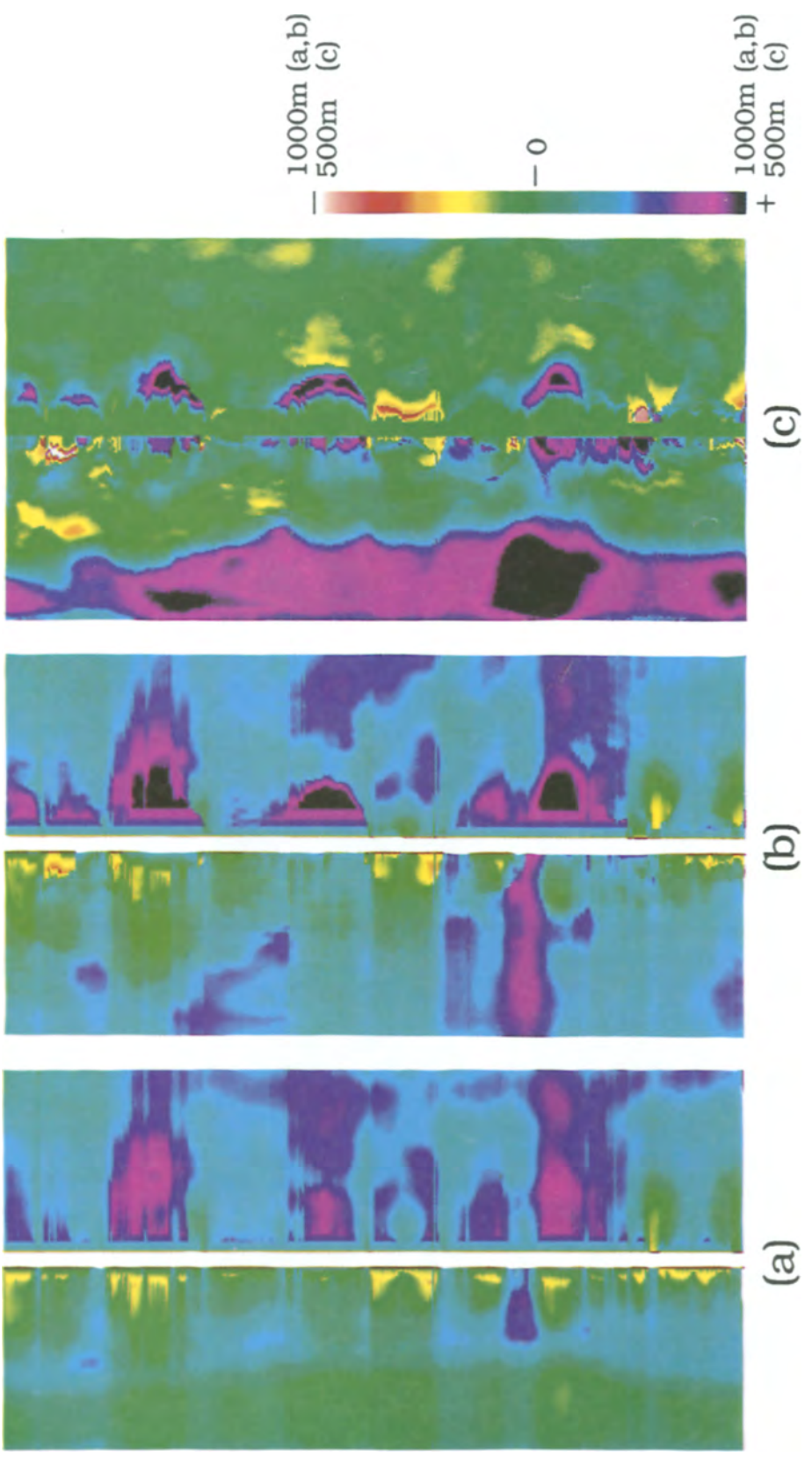

Fig. 14. Extent of pixel migration in the backscatter images shown in Figure 13. Starting from pixel positions given under the flat bottom assumption, the horizontal shifts incurred in the relocation process with (a) SeaMARC II bathymetry or (b) Sea Beam bathymetry, are compared by taking their difference (b)–(a). The color scale bar represents horizontal displacements of ±1000 m for (a) and (b), and ±500 m for their difference.

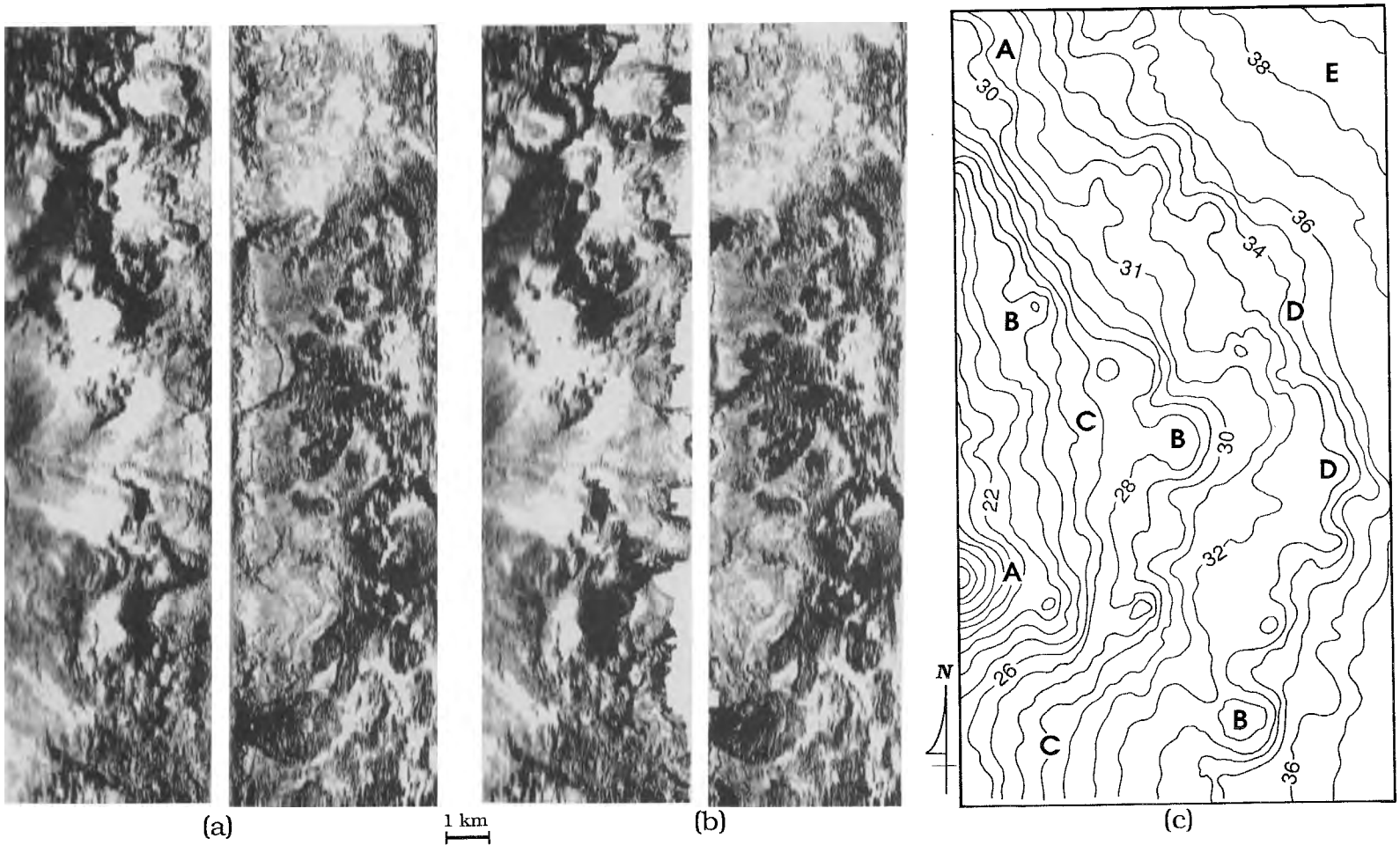

Fig. 15. Navigated image of the middle slope segment of Fieberling Guyot (Figure 10) using (a) the flat bottom assumption, (b) after pixel relocation based on transformed Sea Beam bathymetry, and (c) with contours from the Sea Beam survey, at 100 m interval, matching the relocated pixels of Figure 15b. The letters identify some interpreted geologic features, *viz: A* Rocky spurs, probably built by eruptive radial rift zones, *B* Parasistic lava cones, *C* Sediment-covered talus ramps with downslope bands of high reflectivity that probably mark the most recent, least sedimented rockfall debris, *D* patchy lava outcrops on steep parts of the lower slope, *E* hummocky terrain of slumped sediment below the volcanic slopes.

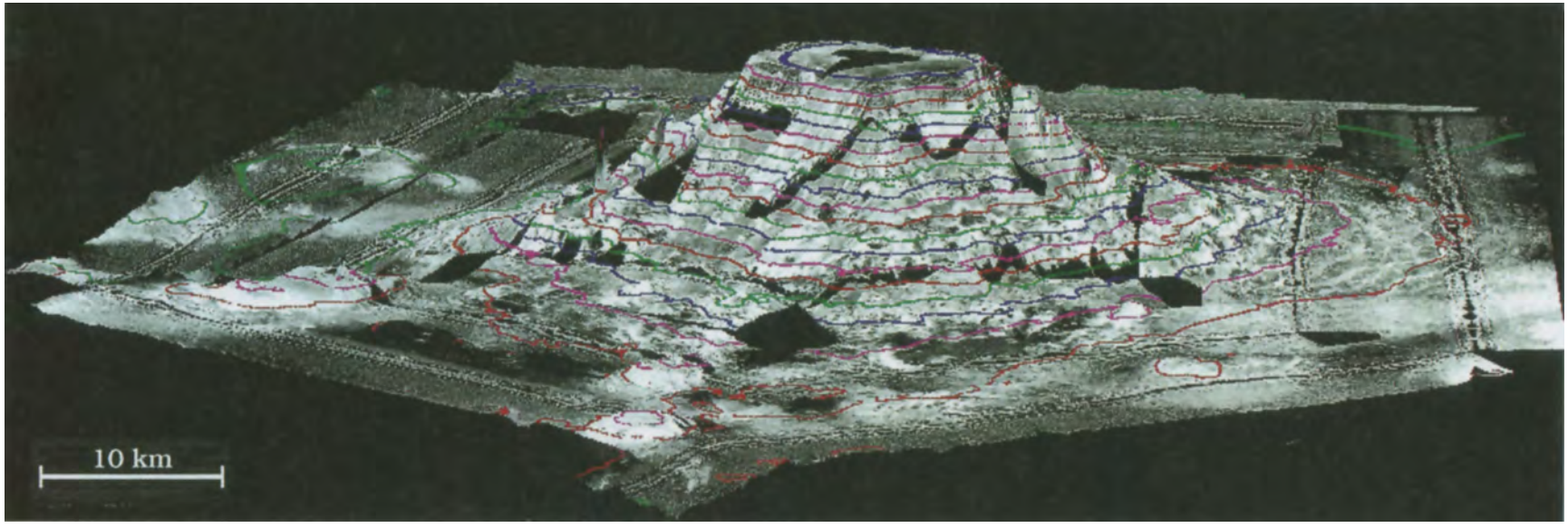

Fig. 16. Perspective view of Fieberling Guyot built from a combination of Sea Beam and SeaMARC II data. The look direction is North with a grazing angle of 15° and a vertical exaggeration of 3.

the central gap can be retained. However, we have chosen to crop the images at nadir to prevent pixels from migrating from one side to the other so as to maintain independence of the two sides of the image that represent different acoustic frequencies (11 kHz on port and 12 kHz on starboard).

The effect of the complete pixel relocation process is displayed in Figure 13b for SeaMARC II bathymetry and in Figure 13c for transformed Sea Beam bathymetry. As described above, the most noticeable changes are found in the central region of the swath where artifacts seen in Figure 13a have been eliminated in Figure 13c, but some artifacts remain in Figure 13b. Likewise, the effect of straight line extrapolation of the SeaMARC II bathymetry, from the last valid sample to the edge of the swath, is well illustrated by the difference in location of features on the outer left side of the swath. Figure 13c is based on the more reliable Sea Beam bathymetry and therefore closer to the true mapping than Figure 13b. This can be verified by merging the backscatter amplitude data with navigation data and by scaling the corresponding raster displays to match the contoured gridded Sea Beam bathymetry as was done in Figure 15.

The navigated backscatter amplitude image (e.g. Figure 15b) can be integrated into a complete mosaic of the survey (Figure 10). Because we have kept the same format for the backscatter amplitude image and for the transformed Sea Beam bathymetry, a similar navigation and scaling process is applied to the bathymetry and the two data sets are co-registered. It is then a simple matter to overlay them and/or to produce perspective views with the backscatter amplitude data draped over the relief (Figure 16).

4. Implication for Geological Interpretation

The salient features of the sidescan mosaic of the whole Guyot (Figure 10) are: (1) low reflectivity of most of the gently sloping summit plain, except for some central rocky areas and a linear target that parallels the rim and is interpreted as a former sea cliff; (2) a complex pattern of high and low reflectivity on the volcano's side slopes; (3) wavy concentric bands of high reflectivity on thick slope-foot sediment lenses which have hummocky surfaces because of progressive slumping; (4) the low reflectivity of most of the surrounding sediment plain, except where it is interrupted by satellite volcanic cones; (5) the lineated north–south pattern of thinly sedimented abyssal hills beyond the sediment plain, seen at the western and eastern margins of Figure 10.

Our procedure for pixel relocation is of greatest benefit to the geological interpreter on the steep side slopes. Comparison of 'before' and 'after' images of part of this terrain (Figure 15a, b) shows gaps in the nearfield on the uphill side where ambiguities, of the type illustrated in Figure 5, exist and have been removed. Artifacts appearing as mirror images near nadir on either side of the track have been properly eliminated, retaining only the primary component. Evidence of feature migration through the relocation process is best illustrated by the easily identifiable sattelite cones that have been shifted several hundred meters, and match their bathymetric expression (Figure 15c). Without knowledge of the bathymetry provided by Sea Beam, the cone lying in the center of the image could not have been detected in Figure 15a, but it was well revealed through the relocation process. Overall, there has been general removal of extraneous and misleading information contained in Figure 15a. In addition, correct positioning of the backscatter amplitude pixels allows them to be accurately registered with the bathymetry, which in turn allows the effect of local relief on backscatter amplitude to be recognized, and distinguished from the effects of varying composition. For example, the lightly shaded areas of Figure 15 have low backscatter either because they are slope facets inclined away from the sonar, as on the backsides of several parasitic cones on the upslope (left) half of the image, or because they have been smoothed with relatively low-reflectivity sediment, as on the talus ramps.

Conclusion

We have shown that several factors must be considered carefully when relocating the pixels in a sidescanned acoustic image of the seafloor by changing the relief representation from the conventional ruled surface with horizontal generating lines at the altitude of the sonar platform, to a more accurate bathymetric surface. (1) The bathymetry must be transformed to reflect the sidescan sonar geometry that constrains slant ranges to increase monotonically athwartships from the first bottom arrival (specular direction), and that produces a beam footprint whose along-track extent widens away from nadir. (2) The spatial resolution or scale of the bathymetry must be commensurate with the general spatial resolution of the image and thus it may not be uniform across-track. Of course, regardless

of scale, the more accurate the bathymetry the better, and we have preferred the Sea Beam bathymetry over that produced by SeaMARC II because of its greater reliability and more complete coverage of the Guyot. Horizontal differences of several hundred meters were found between the relocation resulting from SeaMARC II bathymetry and those obtained using transformed Sea Beam bathymetry.. (3) Geometric corrections are usually done in the athwartships (x, z) plane, however it is sometimes necessary to work in the (x, s) plane to avoid creating unwarranted gaps in the image.

Aside from positioning image features at their correct geographic coordinates, an important benefit of the relocation process is removal from the image of most of the extraneous and misleading information, such as ghost features or ambiguous areas. In addition, the backscatter amplitude data and the bathymetry are fully registered at the end of the process and it is relatively straightforward to display pseudo-3D perspective views of the backscatter amplitude data. With the newer bathymetric sidescan sonar systems that retain the complex waveform for the echoes received, this co-registration is directly obtainable (de Moustier *et al.*, 1991) and integrated bathymetry and acoustic imaging should alleviate the need for much of the post-processing efforts required here. Also, recent advances in multibeam swath bathymetric sonar systems have resulted in the real-time output by these systems of geometrically correct acoustic images of the seafloor (Hammerstad *et al.*, 1991; de Moustier, 1993) in addition to high-resolution bathymetry (rms error of less than 0.35% of water depth) over swaths up to 150° wide. Consequently, for such systems, post-processing efforts will be concentrated on navigation and image processing issues.

Acknowledgements

We thank the Office of Naval Research for supporting this work through grants (N00014-91-J-1073) and (N00014-90-J-4009) under management by the Marine Physical Laboratory and the Hawaii Institute of Geophysics, respectively. We also thank A. N. Shor for his support and Jo Griffith for the art work.

References

Blackinton, J. G., 1986, Bathymetric Mapping with SeaMARC II: An Elevation Angle Measuring Side-Scan Sonar System, Ph.D. dissertation, Hawaii Inst. of Geophys., Univ. of Hawaii, Manoa, 1986.

Carsola, A. J. and Dietz, R. S., 1951, Submarine Geology of Two Flat-Topped Northeast Pacific Seamounts, *American Journal of Science* **250**, 481–497.

Cervenka, P. and de Moustier, C., Post-Processing and Corrections of Bathymetry derived from Sidescan Sonar Systems. Application with SeaMARC II, *IEEE J. Oceanic Eng.* (submitted).

Cervenka, P. and de Moustier, C., 1993, Sidescan Sonar Image Processing Techniques, *IEEE J. Oceanic Eng.* **18**, 108–122.

Hamming, R. W., 1973, Numerical Methods for Scientists and Engineers, chap. 25 to 29, Dover Publications, NY.

Lau, T. K. A. and Fox, C. G., 1991, A Technique for Combining SeaMARC I Sidescan Sonar and Gridded Bathymetry Data to Display Undistorted Seafloor Images, *Proc. IEEE Oceans '91* **2**, 1140–1145.

Lonsdale, P. F., 1991, Structural Patterns of the Pacific Floor Offshore of Peninsular California, *AAPG Memoir* **47**, 87–125.

Mitchell, N. C., 1991, Improving Gloria Images using Sea Beam Data, *J. Geophys. Res.* **96**, 337–351.

de Moustier, C., 1993, Signal Processing for Swath Bathymetry and Concurrent Seafloor Acoustic Imaging, In: *Acoustic Signal processing for Ocean Exploration,* J. M. F. Moura and I. M. G. Lourtie (Eds.), Kluwer Academic Publishers, 329–354.

de Moustier, C., Lonsdale, P. F. and Shor, A. N., 1990, Simultaneous Operation of the Sea Beam Multibeam Echo-Sounder and the SeaMARC II Bathymetric Sidescan Sonar System, *IEEE J. Oceanic Eng.* **15**, 84–94.

de Moustier, C., Masnadi-Shirazi, M. A., and Cervenka, P., 1991, Integrated Processing for Bathymetry and Sidescan Data in Swath Bathymetry Sidelooking Sonars, EOS, *Trans. Am. Geophys. Union* **72**, 249–250.

Hammerstad, E., Pohner, F., Parthiot, F., and Bennett, J., 1991, Field Testing of a New Deep Water Multibeam Echo-Sounder, *Proc. IEEE Oceans '91* **2**, 743–749.

Reed, T. B. and Hussong, D. M., 1989, Digital Image Processing Techniques for Enhancement and Classification of SeaMARC II Sidescan Sonar Imagery, *J. Geophys. Res.* **94**, 7469–7490.

Renard, V. and Allenou, J. P., 1979, Sea Beam Multibeam Echo-Sounding in 'Jean Charcot': Description, Evaluation and First Results, *Int. Hydrog. Rev.* **LVI**(1), 35–67.

Sternlicht, D., 1992, Correcting the Layover Problem: Preprocessing Rectifications for Sidescan Sonar Images, Masters thesis, Univ. Hawaii, Manoa.

Stewart, W. K., 1988, Multisensor Modeling Underwater with Uncertain Information, Ph.D. dissertation, MIT-WHOI.